LOCAL EXPANSION METHOD FOR FAST PLASMA BOUNDARY IDENTIFICATION IN JET

D.P. O'BRIEN, J.J. ELLIS, J. LINGERTAT*
JET Joint Undertaking,
Abingdon, Oxfordshire,
United Kingdom

ABSTRACT. A local expansion technique for the reconstruction of the plasma boundary is presented. The method is particularly accurate in identifying the separatrix in X-point configurations. It is applied to JET discharges and the results are compared with those of a full equilibrium code and with other independent diagnostics. It is found that the majority of the H-mode discharges at JET have been achieved in marginal limiter configurations. The method is sufficiently reliable and fast for real time shape control.

1. INTRODUCTION

The importance of the physical mechanisms, operating at the plasma edge, in determining the overall performance of fusion devices has become increasingly recognized in recent years [1], especially so with the advent of the H-mode high performance regime of operation observed on tokamak machines [2]. The improved confinement region obtained in this mode of operation is known to originate at the plasma edge [3]. Since many of the edge physics diagnostics and models are sensitive to errors in the determination of the plasma boundary, this can lead to contradictory results in the description of the H-mode [4]. Accurate determination of the magnetic field configuration close to the plasma boundary of present day tokamak devices has therefore become increasingly important.

We describe here a local expansion technique to determine the complete plasma boundary. In the past, scepticism has been expressed concerning the use of Taylor series type expansions in global plasma boundary determinations [5–7]. Previously, such expansions have been restricted mostly to a very local region in the vicinity of the measurements, the main application being for plasma position control [8]. The 'local' method used at JET and described here makes use of five 6th order expansions of the flux function which are symmetric in major radius and constrained by the vacuum field equations. By fitting to the local field and flux measurements they can give an accurate determination of the boundary in the vicinity of the measurements. The expansion in the region of an X-point for separatrix configurations is particularly suitable in localizing the X-point. By constraining adjoining fits to match at chosen 'tie' points, a global reconstruction of the plasma boundary is obtained. In line with the philosophy of the method, these constraints are applied in a least squares sense. The method is sufficiently reliable and fast for real time shape control.

2. LOCAL EXPANSION TECHNIQUE

The local expansion method was originally introduced at JET in order to have a fast and accurate determination of the plasma boundary in the neighbourhood of an X-point. This method has been extended to cover the whole plasma boundary and is now used for arbitrary plasma configurations. The basis of the method is five 6th order expansions of the poloidal flux, one each at the top, bottom, inboard, upper belt and lower belt limiters of the vessel. The expansions are given by

$$\psi(R,Z) = \sum_{\substack{i=0 \\ j=0 \\ i+j\le 6}}^{6} a_{ij}\rho^i z^j \qquad (1)$$

where $\rho = R^2 - R_0^2$, $z = Z - Z_0$, and (R_0, Z_0) is the centre of the expansion. The variable ρ rather than $R - R_0$ is chosen because of the symmetry of the Grad–Shafranov equation about the major axis of the torus ($R = 0$). The coefficients a_{ij} are determined by imposing the vacuum equation

$$\Delta^*\psi = 0\,; \quad \Delta^* = \partial_{RR} + \partial_{ZZ} - \frac{1}{R}\partial_R \qquad (2)$$

* Max-Planck-Institut für Plasmaphysik, Garching, Germany.

and by fitting to the local flux and magnetic field measurements. In addition, the five expansions are constrained to match at chosen tie points around the vessel.

Having imposed the vacuum equation, each expansion is left with 13 independent coefficients to be determined, leading to a total number of 65 coefficients for the five expansions. The flux and magnetic field can be written in terms of these coefficients as

$$\psi_c^\alpha(\rho,z) = \sum_{i=1}^{13} \psi_i^\alpha(\rho,z)\, C_i^\alpha$$
$$B_c^\alpha(\rho,z) = \sum_{i=1}^{13} B_i^\alpha(\rho,z)\, C_i^\alpha \qquad \alpha = 1 \ldots . 5 \tag{3}$$

where B_c refers to the component of B in the direction of the measuring coil. If no ties between the expansions are used, each fit is independent, giving rise to five least squares calculations from minimizing

$$\chi_\alpha^2 = \tfrac{1}{2} \sum_{\substack{Flux \\ loops}} \mathrm{w_j^\alpha} \left(\psi_m^\alpha(\mathrm{j}) - \psi_c^\alpha(\mathrm{j})\right)^2 + \tfrac{1}{2} \sum_{coils} \mathrm{w_j^\alpha} \left(B_m^\alpha(\mathrm{j}) - B_c^\alpha(\mathrm{j})\right)^2 \tag{4}$$

with respect to the C_i^α, where (ψ_m, B_m) and (ψ_c, B_c) are the measured and calculated values of the flux and field at the measuring points (R_j, Z_j). The weighting factor w_j^α describes the expected accuracy of the measurements. The five fits can be combined to the equivalent minimization of

$$\chi^2 = \tfrac{1}{2} \sum_{\mathrm{j}=1}^{N_m} \mathrm{w_j} \left(m_j - \sum_{i=1}^{65} d_{\mathrm{ji}} C_i\right)^2 \tag{5}$$

where m_j are the measurements and $d_{ij} \equiv \psi_i^\alpha(\rho_j, z_j)$, etc. For each j, only 13 of the d_{ij} are non-zero. Each physical measurement may occur in more than one expansion, so the m_j are not necessarily distinct. The minimization can be summarized as

$$DC = M^* \tag{6}$$

where

$$D_{ki} = \sum_{\mathrm{j}=1}^{Nm} \mathrm{w_j}\, d_{\mathrm{ji}}\, d_{jk}$$
$$M_k^* = \sum_{\mathrm{j}} \mathrm{w_j}\, d_{\mathrm{jk}}\, m_{\mathrm{j}} \tag{7}$$

We see that D consists of five 'diagonal blocks' of 13×13 matrices $D(\alpha)$ of the form

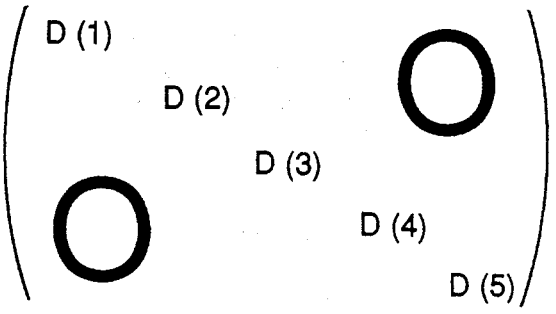

The choice of 6th order for the expansion and the use of five fits is a compromise. The accuracy of the results (judged by comparison with an equilibrium code) improved as the order of the expansion and the number of fits was raised, but the required number of measurements also increased. The truncation errors associated with a Taylor expansion become worse as the distance from the centre of the expansion increases, and so the use of measurements far from $\rho = 0$, $z = 0$ in the least squares fit results in a decrease in the accuracy of the answer. To overcome this problem, additional constraints were introduced between neighbouring expansions such that the fluxes at given points were made to agree. These 'tie' points were chosen midway between the expansion centres (where the errors from the two expansions are comparable), in groups of four (to match the flux and its derivative, the magnetic field), and in a region outside the plasma. By this means the maximum distance of a measurement from the corresponding centre could be reduced. Initially neighbouring expansions were constrained to agree exactly at these 'hard tie points'.

It was found that the results could be improved (especially with small plasmas) by relaxing the constraint that adjacent expansions match exactly, but allowing an error term $w_j\ (\psi^\alpha(R_j, Z_j) - \psi^\beta(R_j, Z_j))^2$ to be included in the expression to be minimized. These so-called soft ties between the fits are implemented by introducing additional measurements $m_j = 0$ at points (R_j, Z_j) where the ties are to be imposed and defining additional matrix elements $d_{ij} \equiv d(1)_{ji} - d(2)_{ji}$, where i is the coefficient index, j labels the tie point (R_j, Z_j), and $d(1)$, $d(2)$ refer to the two fits involved in the tie. This procedure introduces non-zero off-diagonal blocks into the block matrix D described above; the method of solution remains the same, but a 65×65 matrix must now be inverted.

When inaccurate data are suspected, hard ties are introduced in order to constrain two neighbouring fits

to match exactly at a point (R_j, Z_j). A constraint between fits 1 and 2 would have the form

$$\sum_{i=1}^{65} d_{ji}(1)C_i = \sum_{i=1}^{65} d_{ji}(2)C_i \quad (8)$$

Hence, each hard tie point allows one of the 65 coefficients to be eliminated from the calculation, so that we can write

$$AC^h = BC^r \quad (9)$$

where the 65 coefficients C are divided into n_h coefficients C^h, which are eliminated from the minimization process, and $65 - n_h$ coefficients C^r. The coefficients in C^h are chosen so that A is non-singular, giving

$$C^h = A^{-1}BC^r \quad (10)$$

and a matrix T can be constructed where

$$C = TC^r$$

If we substitute this expression for C into χ^2 and minimize with respect to C^r, this is equivalent to replacing

$$\sum_{i=1}^{65} d_{ji}\, C_i \text{ by } \sum_{i=1}^{65-n_h} d^*_{ji}\, C^r_i$$

where

$$d^*_{ji} = \sum_{k=1}^{65} d_{ji}\, T_{ki}.$$

This leads to a minimization given by an equation of the type (6).

Without any tie point constraints, each expansion requires at least 13 measurements to give a solution. At present, the JET magnetic measurement system just about satisfies these criteria. There are plans to increase the number of available measurements, which will give a more robust reconstruction. The plasma boundary is found in the usual way by finding the minimum flux value (the plasma current in JET is negative) between various limiter components around the vessel as well as at any separatrices if they exist inside the vessel. Any X-points of the poloidal field B_p are found using a Newton–Raphson procedure to solve $\nabla\psi = 0$. As with most other methods, any significant currents flowing outside the separatrix or in the vacuum vessel will reduce the accuracy of the answer.

3. BENCHMARK CALCULATIONS

In order to benchmark the method, we reconstruct the plasma boundary for various plasma configurations, using magnetic data generated by the full equilibrium

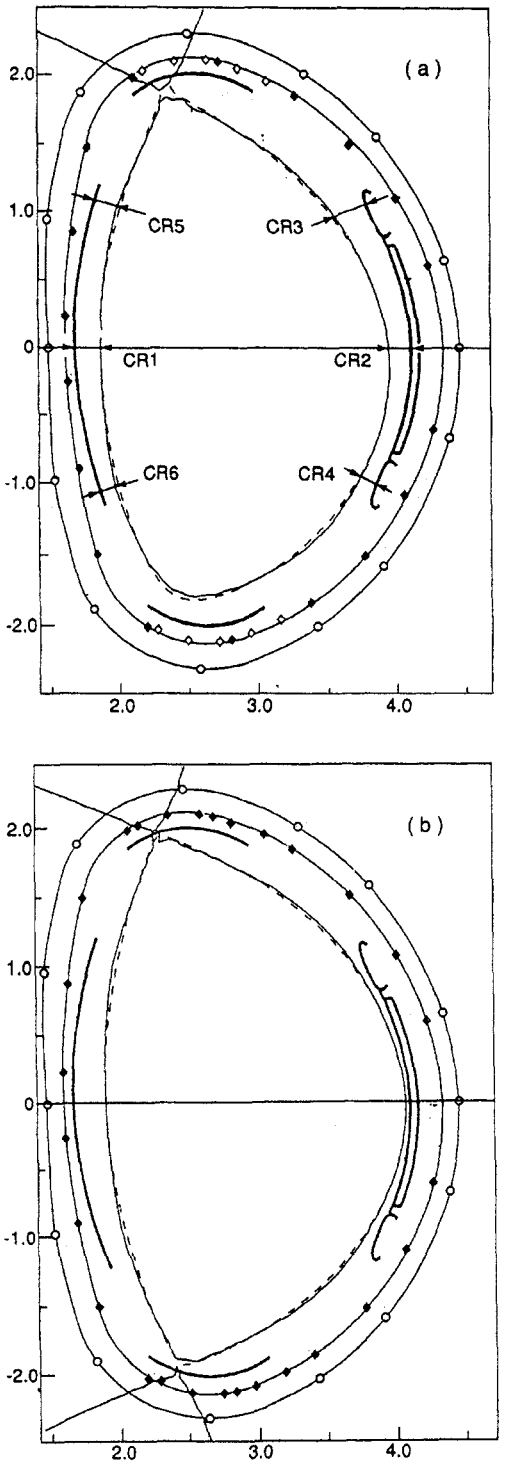

FIG. 1. (a) XLOC boundary (thick solid curve) superimposed on the IDENTC boundary for a single null X-point configuration. Also shown are the distances CR1–CR6 to various components of the vessel. The diamonds and the circles give the positions of the magnetic field and flux measurements, respectively. Open diamond symbols indicate positions where two directions of the field are measured.
(b) XLOC boundary (thick solid curve) superimposed on the IDENTC boundary for a double-null X-point configuration.

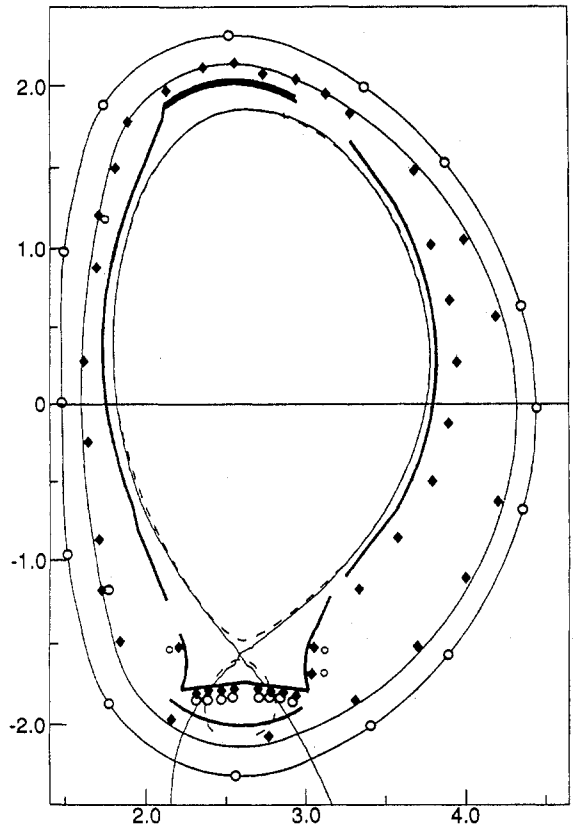

FIG. 2. XLOC boundary (thin solid curve) superimposed on the EFITJ boundary for a 5 MA fat pumped divertor configuration.

code IDENTC [9]. The usual magnetic field measurements at JET are used. They consist of a maximum of 34 magnetic coils and 14 flux loops placed around the wall of the vessel. There is a higher density of magnetic coils at the top and bottom of the vessel in regions where X-points of the field are formed. In these regions we also measure two perpendicular components of the magnetic field in order to give a more accurate location for X-points.

Figure 1 presents a comparison between the numerically generated boundaries of IDENTC and the reconstructed boundaries using the local expansion method XLOC. We see that for all configurations there is good agreement, with an error of less than 2% (~2 cm) of the minor radius for the whole boundary. Given that the grid size in IDENTC is of the order of 7 cm, this discrepancy could easily be absorbed into the inaccuracy of the numerical scheme underlying IDENTC.

For the proposed pumped divertor, which will become operational in 1993 [10], we reconstruct the plasma boundary using magnetic data generated by the full equilibrium code EFITJ [11]. The magnetic field measurements are now 44 magnetic coils and 27 flux loops. The comparison between the EFITJ boundary and the reconstructed boundary using XLOC is shown in Fig. 2.

4. EXPERIMENTAL RESULTS

The local expansion method of plasma boundary reconstruction has been run continuously during operations at JET for the past three years. We have extracted data from the JET database system in order to make comparisons with other boundary diagnostics. The results are presented below.

4.1. Comparison with IDENT

The distances CR1-CR6 used to characterize the plasma boundary are shown in Fig. 1(a). They are respectively the distance to the inner wall, the RF antenna, the upper belt limiter, the lower belt limiter, the upper inner wall and the lower inner wall. Figure 3 presents a comparison of these distances between the reconstructed boundary from XLOC and the reconstructed boundary from IDENTC, in the form of a scatter plot, using data from the 1990–1992 JET experimental campaigns. We see that there is generally good agreement, especially when the plasma to vessel component distance is less than 10 cm.

4.2. Comparison with independent diagnostics

The standard interpretation of the divertor diagnostics uses the magnetic configuration given by XLOC in the divertor region. However, for some discharges it is possible to use raw measurements from these diagnostics to check the accuracy of XLOC. The divertor diagnostics used for this purpose are the Langmuir probes installed in the target plates and the CCD camera recordings of the light emission from the target plates.

If the X-point of a discharge is swept across the target tiles so that the strike points of the separatrix cross over a Langmuir probe, changes in the Langmuir characteristics will result. Although the detailed physics of the rapid changes in the plasma parameters that occur at the transition between the scrape-off layer and the private flux region are not fully understood, it is reasonable to assume that the transition takes place where the major changes in the Langmuir characteristics occur. Figure 4 shows the radial position of the inner and outer magnetic

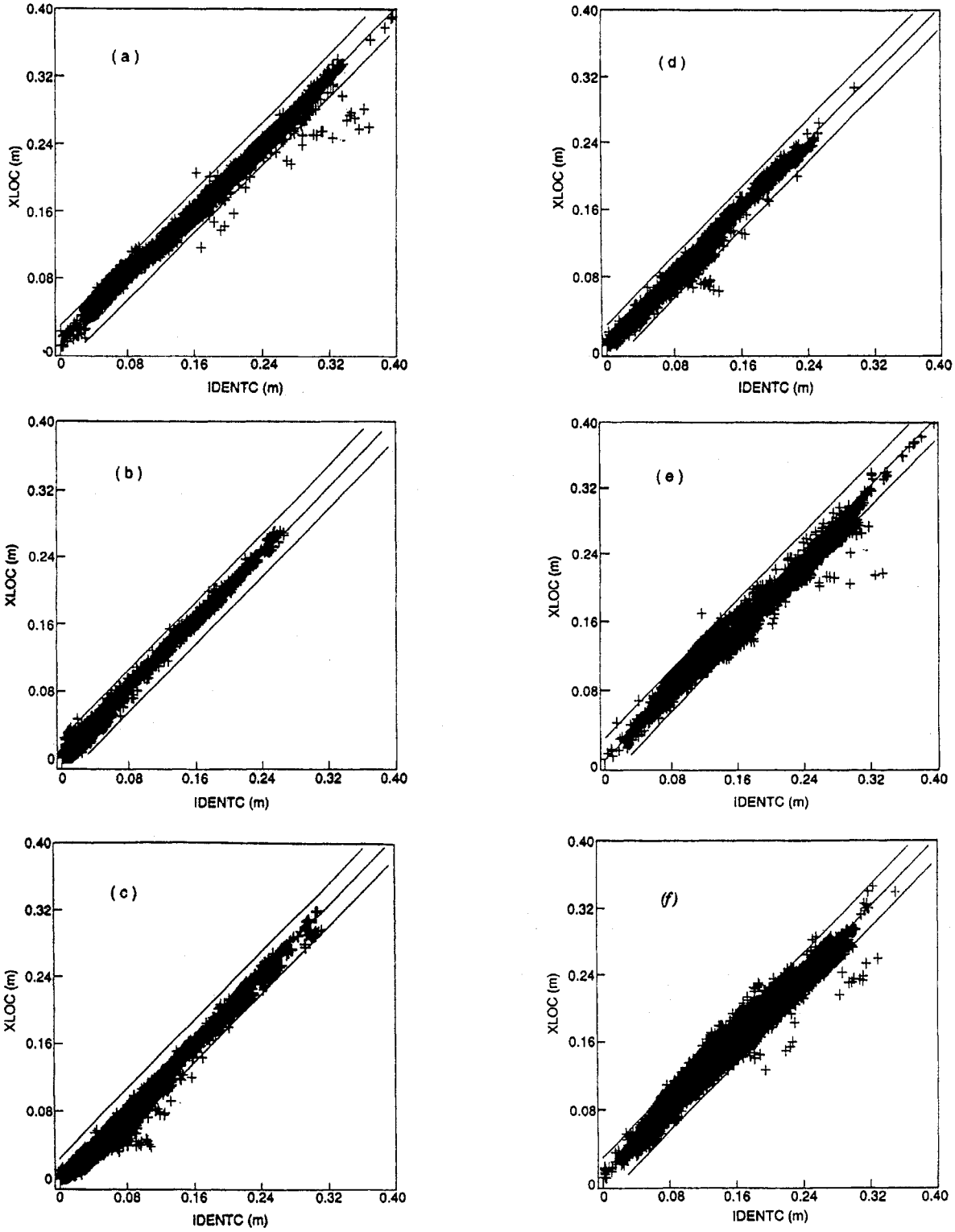

FIG. 3. (a) Plasma inner wall distance from XLOC versus the corresponding IDENTC distance for pulses during the 1990–1992 JET campaigns. The lines represent $y = x$, $y = x + 2$ cm and $y = x - 2$ cm. (b) Plasma RF antenna distance from XLOC versus the corresponding IDENTC distance for pulses during the 1990–1992 JET campaings. (c) Plasma upper belt distance from XLOC versus the corresponding IDENTC distance for pulses during the 1990–1992 JET campaigns. (d) Plasma lower belt distance from XLOC versus the corresponding IDENTC distance for pulses during the 1990–1992 JET campaigns. (e) Plasma upper inner wall distance from XLOC versus the corresponding IDENTC distance for pulses during the 1990–1992 JET campaigns. (f) Plasma lower inner wall distance from XLOC versus the corresponding IDENTC distance for pulses during the 1990–1992 JET campaigns.

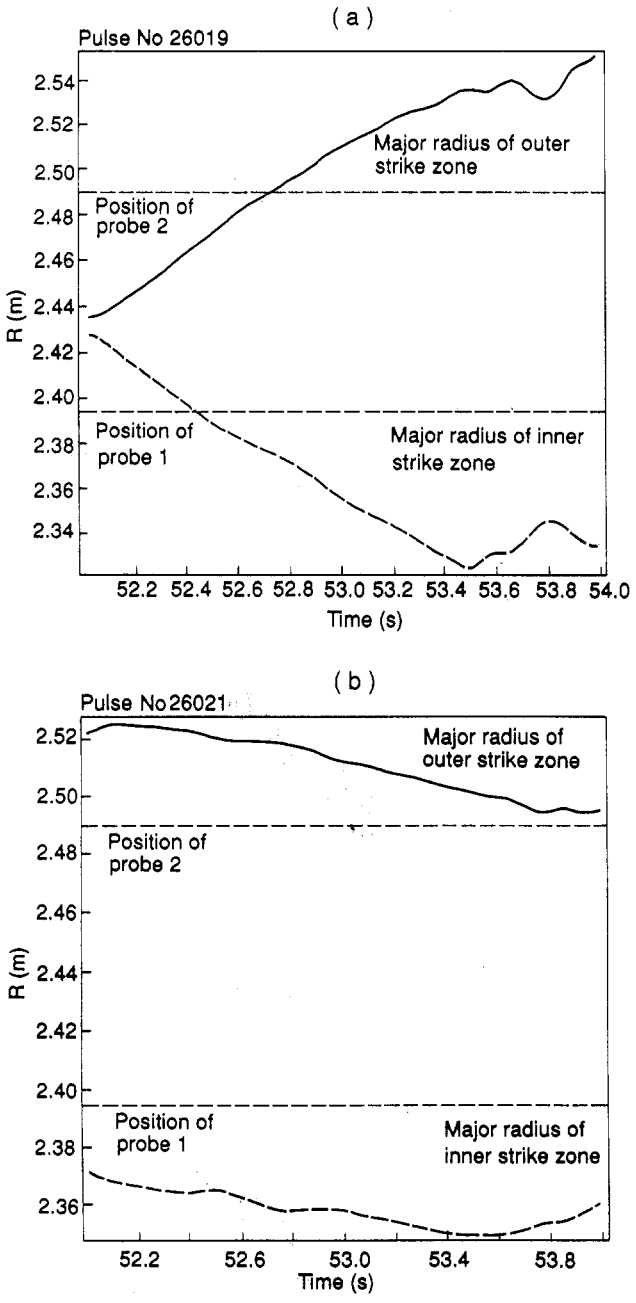

FIG. 4. (a, b) Major radius of the inner and outer strike points of the separatrix calculated by XLOC, as a function of time, with the positions of Langmuir probes 1 and 2 marked for shots 26019 and 26021, respectively.

strike points given by XLOC as a function of time for two hot-ion upper X-point discharges. The radial position of two probes is also given. According to Fig. 4, both probes are crossed by both strike points for shot 26019, whereas only probe 2 is approached for shot 26021. Figures 5 and 6 show the floating potential U_f of the probes as a function of the strike point position R_{XLOC}. The floating potential is an unprocessed parameter taken directly from the measured Langmuir characteristics. We see that there is a clear and distinct change of the floating potential within a narrow region ΔR_{XLOC} of the major radius (ΔR_{XLOC} = 5–12 mm). It is assumed that this change is the result of the strike

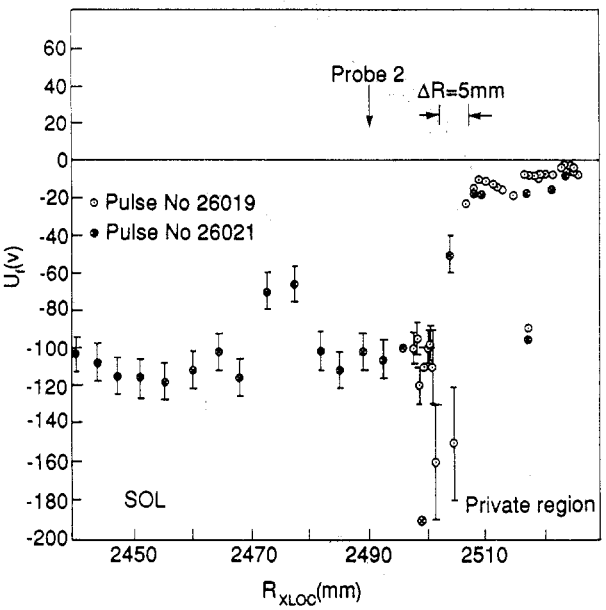

FIG. 5. Floating potential U_f at probe 2, plotted as a function of the position of the outer strike point calculated by XLOC for shots 26019 and 26021.

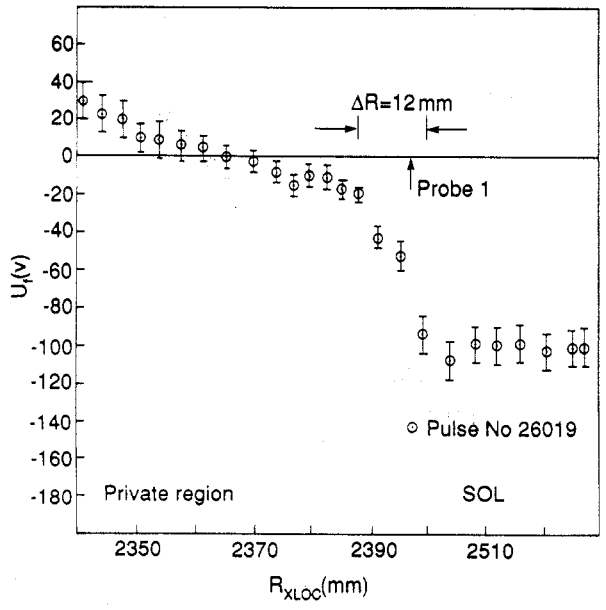

FIG. 6. Floating potential U_f at probe 1, plotted as a function of the position of the inner strike point calculated by XLOC for shot 26019.

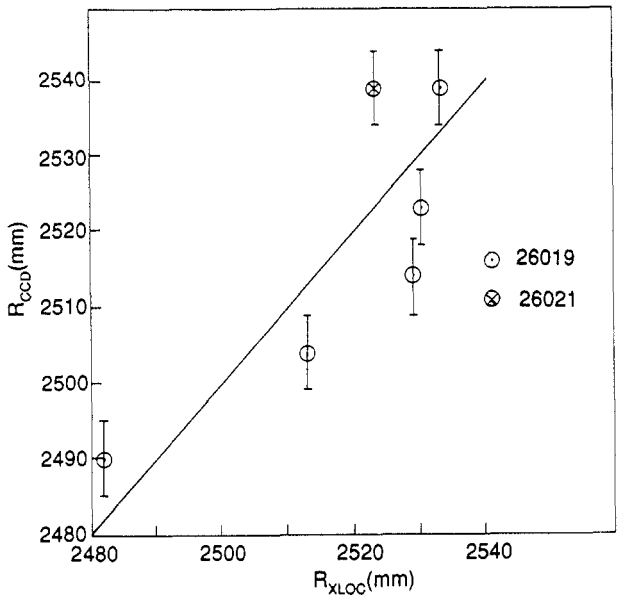

FIG. 7. Location of the outer strike zone determined from the CCD camera recordings versus the calculated outer strike point position from XLOC.

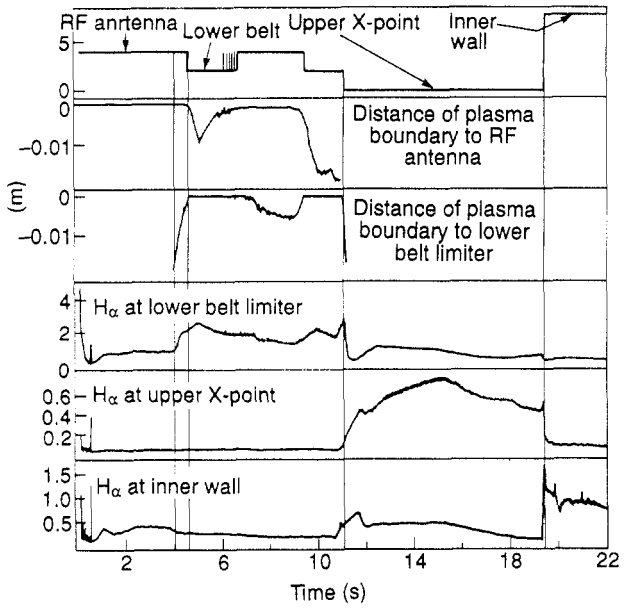

FIG. 8. Comparison of the XLOC plasma configuration with spectroscopic measurements.

point crossing over the respective probe. This assumption is supported by the fact that the plasma parameters obtained after processing the Langmuir characteristics (n_e, T_e) undergo similar changes in the same interval ΔR.

On the CCD camera recordings of the light emission from the target plates, very well localized hot spots can be observed. Generally, they are located on tiles that have a larger inclination against the magnetic field than the flat surface of the plates. The location of the hot spots should be at the maximum of the parallel heat flux, i.e. just at the strike points of the separatrix [12]. From the tape recordings of shots 26019 and 26021 the radial co-ordinate R_{CCD} of the hot spot at the outer strike points was visually determined relative to geometric features of the target tiles (edges, bolt holes). This method was used only in time intervals where the radial width of the hot spot was less than 1 cm; the estimated accuracy of this procedure is $\pm$ 1 cm. The values obtained, together with the corresponding radial position of the strike point according to XLOC, R_{XLOC}, are given in Fig. 7, which shows a scatter of the measured points around the straight line of ideal agreement between the two methods. The maximum deviation from the straight line is 16 mm and the mean deviation is 10 mm. These methods give comparable values of accuracy ($\pm$10 mm) for XLOC. The Langmuir probe results show a systematic difference

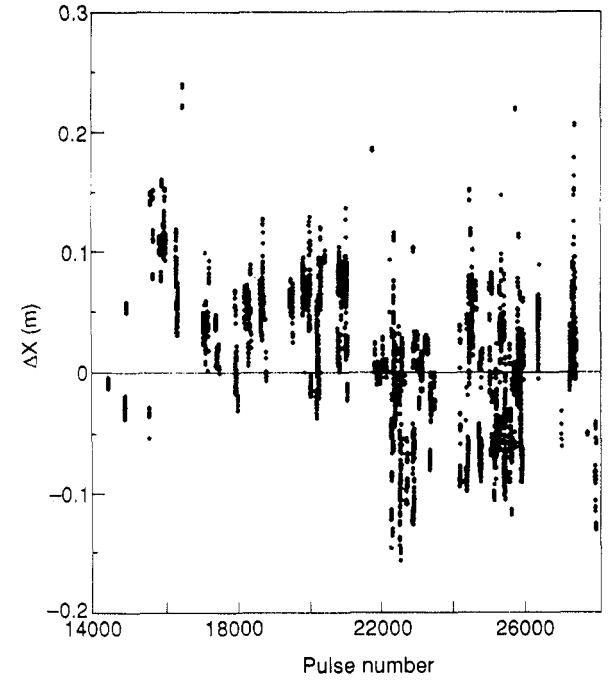

FIG. 9. Distance of the upper X-point from the carbon tiles for H-mode discharges during the 1988–1992 JET campaigns. A positive value corresponds to X-points outside the vessel and a negative value to X-points inside the vessel.

between XLOC and the positions of the probe, whereas the CCD results show a random scatter. It seems that the assumed accuracy of the CCD method is overestimated and that the Langmuir probe results are more representative. CCD camera recordings of five lower X-point discharges with varying distance between the X-point and the target plate (ΔX = 2, 3, 8 and 13 cm) were also analysed. The results obtained confirm the findings in the above mentioned upper X-point shots (ΔX = 9 and 11 cm). The maximum deviation between R_{XLOC} and R_{CCD} is within the accuracy of the method ($\pm$10 mm).

Spectroscopy measurements can also be used to assess the accuracy of the boundary reconstruction. As the plasma changes configuration from outboard limiter to divertor to inner wall limiter, the neutral H flux as measured by the H_α bremsstrahlung in these positions rises and falls accordingly. Figure 8 shows the configuration obtained by XLOC as a function of time (RF antenna limiter = 4, lower belt limiter = 2, upper X-point = 0, inner wall limiter = 8), with the various H_α signals plotted beneath. We see that the transitions from RF antenna to lower belt limiter and from RF antenna to lower belt limiter to upper X-point to inner wall, obtained by XLOC, are simultaneous with the variations in the H_α signals in the appropriate regions. This corresponds to an accuracy of less than 1 cm for the magnetic boundary reconstruction at the inboard and outboard limiters of the vessel.

4.3. H-mode

The results obtained from XLOC for the position of the X-point showed that before the end of 1990, most of the H-modes achieved at JET were 'marginally limited', with the X-point outside the vessel and the plasma limited on the carbon tiles in the divertor region. Subsequently, magnetic configurations were obtained with the X-point well inside the vessel. These results are summarized in Fig. 9. The effect of the X-point position on confinement is discussed in Ref. [13], the main conclusion being that the diamagnetic stored energy scales with I_p more weakly than linearly as the X-point moves further outside of the vessel with increasing current.

5. SUMMARY

The XLOC boundary reconstruction package is in routine use at JET and has an accuracy in localizing X-points of <2 cm. Its boundary has been compared with the boundary of the full equilibrium identification code IDENTC, showing excellent agreement at the inboard and outboard sides of the plasma. However, it gives a more accurate X-point location when comparisons are made with other diagnostics such as the Langmuir probes in the X-point region and the strike zones obtained from the CCD camera observations. This more accurate determination of the X-points has shown that H-modes at JET can be obtained with a marginally limited configuration as well as in true X-point configurations with the X-point inside the vessel.

ACKNOWLEDGEMENTS

The authors would like to thank Prof. K. Lackner, Dr. J.G. Cordey and Dr. J.P. Christiansen for stimulating discussions. They would also like to thank M. Lesourd who provided the CCD camera observations.

REFERENCES

[1] STANGEBY, P.C., McCRACKEN, G.M., Nucl. Fusion **30** (1990) 1225.
[2] WAGNER, F., BARTIROMO, R., BECKER, G., et al., Nucl. Fusion **25** (1985) 1490.
[3] ASDEX Team, Nucl. Fusion **29** (1989) 1959.
[4] HARBOUR, P.J., LOARTE, A., CLEMENT, S., A new approach to scaling of the scrape off layer and divertor plasma in JET, to be published in J. Nucl. Mater.
[5] LEE, D.K., PENG, Y., PENG, K.M., Plasma Phys. **25** (1981) 161.
[6] BRAAMS, B.J., The Interpretation of Tokamak Magnetic Diagnostics. Status and Prospects, Rep. IPP 5/2, Max-Planck-Institut für Plasmaphysik, Garching (1985).
[7] HOFMANN, F., TONETTI, G., Nucl. Fusion **28** (1988) 519.
[8] BERTOLINI, E., MONDINO, P., NOLL, C.P., Fusion Technol. **11** (1987) 71.
[9] BLUM, J., LAZZARO, E., O'ROURKE, J. KEEGAN, B., STEPHAN, Y., Nucl. Fusion **30** (1990) 1475.
[10] REBUT, P.H., LALLIA, P.P., Workshop on the New Phase for JET: The Pumped Divertor Proposal, Rep. JET-R (89) 16, JET Joint Undertaking, Abingdon, Oxfordshire (1989) 1.
[11] O'BRIEN, D.P., KOVANEN, M.A., REICHLE, R., et al., in Controlled Fusion and Plasma Heating (Proc. 17th Eur. Conf. Amsterdam, 1990), Vol. 14B, Part I, European Physical Society (1990) 251.
[12] LOARTE, A., HARBOUR, P.J., Nucl. Fusion **32** (1992) 681.
[13] JONES, T.T.C., BALET, B., BRUSATI, M., et al., in Controlled Fusion and Plasma Physics (Proc. 19th Eur. Conf. Innsbruck, 1992), Vol. 16C, Part I, European Physical Society (1992) 681.

(Manuscript received 10 August 1992
Final manuscript received 23 December 1992)